# REPORT DOCUMENTATION PAGE

Form Approved OMB NO. 0704-0188

The public reporting burden for this collection of information is estimated to average 1 hour per response, including the time for reviewing instructions, searching existing data sources, gathering and maintaining the data needed, and completing and reviewing the collection of information. Send comments regarding this burden estimate or any other aspect of this collection of information, including suggesstions for reducing this burden, to Washington Headquarters Services, Directorate for Information Operations and Reports, 1215 Jefferson Davis Highway, Suite 1204, Arlington VA, 22202-4302. Respondents should be aware that notwithstanding any other provision of law, no person shall be subject to any oenalty for failing to comply with a collection of information if it does not display a currently valid OMB control number.
PLEASE DO NOT RETURN YOUR FORM TO THE ABOVE ADDRESS.

| 1. REPORT DATE (DD-MM-YYYY) | 2. REPORT TYPE | 3. DATES COVERED (From - To) |
|---|---|---|
| 23-07-2015 | Conference Proceeding | - |

4. TITLE AND SUBTITLE

Towards direct simulations of counterflow flames with consistent differential-algebraic boundary conditions

5a. CONTRACT NUMBER
W911NF-11-1-0398

5b. GRANT NUMBER

5c. PROGRAM ELEMENT NUMBER
611102

6. AUTHORS

Panayotis D. Kourdis, Josette Bellan, Kenneth Harstad

5d. PROJECT NUMBER

5e. TASK NUMBER

5f. WORK UNIT NUMBER

7. PERFORMING ORGANIZATION NAMES AND ADDRESSES

California Institute of Technology
1200 E. California Blvd.

Pasadena, CA 91125 -0001

8. PERFORMING ORGANIZATION REPORT NUMBER

9. SPONSORING/MONITORING AGENCY NAME(S) AND ADDRESS (ES)

U.S. Army Research Office
P.O. Box 12211
Research Triangle Park, NC 27709-2211

10. SPONSOR/MONITOR'S ACRONYM(S)
ARO

11. SPONSOR/MONITOR'S REPORT NUMBER(S)
58744-EG.13

12. DISTRIBUTION AVAILIBILITY STATEMENT

Approved for public release; distribution is unlimited.

13. SUPPLEMENTARY NOTES

The views, opinions and/or findings contained in this report are those of the author(s) and should not contrued as an official Department of the Army position, policy or decision, unless so designated by other documentation.

14. ABSTRACT

A new approach for the formulation of boundary conditions for the counterflow configuration is presented. Upon discretization of the steady-state Navier-Stokes equations at the inflow boundaries, numerically algebraic equations are imposed as boundary conditions, while upon discretization of the unsteady Navier-Stokes equations at the outflow, differential boundaries result. It is demonstrated that the resulting numerical differential-algebraic boundary conditions are suitable to account for the multi-directional character of the flow at the boundaries of the counterflow configuration.

15. SUBJECT TERMS

simulations of counterflow laminar flames

| 16. SECURITY CLASSIFICATION OF: | | | 17. LIMITATION OF ABSTRACT | 15. NUMBER OF PAGES | 19a. NAME OF RESPONSIBLE PERSON |
|---|---|---|---|---|---|
| a. REPORT | b. ABSTRACT | c. THIS PAGE | | | Josette Bellan |
| UU | UU | UU | UU | | 19b. TELEPHONE NUMBER: 818-354-6959 |

## Report Title

Towards direct simulations of counterflow flames with consistent differential-algebraic boundary conditions

## ABSTRACT

A new approach for the formulation of boundary conditions for the counterflow configuration is presented. Upon discretization of the steady-state Navier-Stokes equations at the inflow boundaries, numerically algebraic equations are imposed as boundary conditions, while upon discretization of the unsteady Navier-Stokes equations at the outflow, differential boundaries result. It is demonstrated that the resulting numerical differential-algebraic boundary conditions are suitable to account for the multi-directional character of the flow at the boundaries of the counterflow configuration.

**Conference Name:** Aerospace Sciences Meeting

**Conference Date:** January 05, 2015

# Towards direct simulations of counterflow flames with consistent differential-algebraic boundary conditions

Panayotis D. Kourdis *

*Mechanical and Civil Engineering Dept., California Institute of Technology, Pasadena, CA 91125, USA*

Josette Bellan †

*Jet Propulsion Laboratory, California Institute of Technology, Pasadena, CA 91109, USA*

*Mechanical and Civil Engineering Dept., California Institute of Technology, Pasadena, CA 91125, USA*

Kenneth Harstad ‡

*Jet Propulsion Laboratory, California Institute of Technology, Pasadena, CA 91109, USA*

**A new approach for the formulation of boundary conditions for the counterflow configuration is presented. Upon discretization of the steady-state Navier-Stokes equations at the inflow boundaries, numerically algebraic equations are imposed as boundary conditions, while upon discretization of the unsteady Navier-Stokes equations at the outflow, differential boundaries result. It is demonstrated that the resulting numerical differential-algebraic boundary conditions are suitable to account for the multi-directional character of the flow at the boundaries of the counterflow configuration.**

## I. Introduction

The counterflow configuration provides a comprehensive framework for studying the characteristics of non-premixed laminar and turbulent flame problems[1–6]. However, apart from the simplified one-dimensional spatial models, the fidelity of direct numerical simulations (DNSs) for the counterflow configuration in terms of robustness/accuracy exhibit significant sensitivity to the boundary condition (BC) treatment[7–9]. This behavior is mainly due to the multi-directional character of the flow at the boundaries which must be properly accounted by the BCs. To mitigate this problem, Yoo et al.[7] developed improved BCs based on the Navier-Stokes Characteristic Boundary Conditions[10] (NSCBCs) for laminar and turbulent counterflow flames. The major improvement consisted in introducing the (no-longer negligible) transverse terms into the Locally One Dimensional Inviscid (LODI) relations in order to capture the multi-dimensional effects at the inflow/outflow boundaries. However, two major shortcomings can also be identified with the improved NSCBCs. First, they preserve the use of relaxation coefficients entering the improved LODI relations and these coefficients are problem specific. These coefficients provide an optimal balance between achieving the prescribed upstream values for the inflow variables and reducing spurious wave reflections, and usually must be determined through a trial and error process; this is an expensive, time-consuming procedure. Second, once derived for real-gas, the implementation of these revised NSCBCs adds a considerable computational cost.

In this work, we adopt a totally different viewpoint for constructing BCs for the counterflow configuration that results in a very concise framework. In particular, we combine the steady-state Navier-Stokes equations with an initial flow of potential type to construct numerically consistent algebraic BCs at the inflow boundaries. The structure of the paper is as follows. First, the governing equations of the problem are presented. A detailed discussion on the construction of the initial profile of the flow follows. Then, the new BCs are provided for the inflow and outflow boundaries. The specifics regarding the numerical implementation that was

*Caltech Postdoctoral Scholar, AIAA Member.

†Senior Research Scientist, AIAA Fellow (Corresponding Author. Email: josette.bellan@jpl.nasa.gov).

‡Senior Engineer.

employed follows. Next, the validation of the proposed differential-algebraic BCs with numerical examples is performed. Finally, a summary is given and several aspects regarding the proposed approach are discussed.

## II. Governing equations

### A. The Navier-Stokes equations

The Navier-Stokes (NS) equations for a compressible reacting multicomponent mixture of $N$ species expressed in terms of the conservative variables $\widetilde{\mathbf{U}} = [\widetilde{U}_m]\,(m = 1, \ldots, N+4)$ where

$$\widetilde{\mathbf{U}} \equiv [\rho, \rho u_1, \rho u_2, \rho u_3, \rho Y_1, \ldots, \rho Y_{N-1}, \rho e_t]^T \tag{1}$$

and in Cartesian coordinates are

$$\frac{\partial \rho}{\partial t} + \frac{\partial (\rho u_j)}{\partial x_j} = 0 \tag{2}$$

$$\frac{\partial (\rho u_i)}{\partial t} + \frac{\partial (\rho u_i u_j)}{\partial x_j} + \frac{\partial p}{\partial x_i} = \frac{\partial \tau_{ij}}{\partial x_j} \quad (i, j = 1, 2, 3) \tag{3}$$

$$\frac{\partial (\rho Y_n)}{\partial t} + \frac{\partial (\rho Y_n u_j)}{\partial x_j} = -\frac{\partial J_{nj}}{\partial x_j} + \dot{\omega}_n \quad (n = 1, \ldots, N-1) \tag{4}$$

$$\frac{\partial (\rho e_t)}{\partial t} + \frac{\partial [(\rho e_t + p) u_j]}{\partial x_j} = -\frac{\partial q_j}{\partial x_j} + \frac{\partial (\tau_{ij} u_i)}{\partial x_j} \tag{5}$$

where the indices $i$ and $j$ follow the summation convention, $t$ is time, $x_j$ is the $j$-th spatial coordinate, $\rho$ is the mass density of the fluid, $u_j$ is the $j$-th component of the velocity vector, $Y_n$ is the mass fraction of species $n$, $p$ is the pressure, $e_t = e + \frac{1}{2} u_i u_i$ is the total specific energy ($e$ stands for the specific internal energy), $J_{nj}$ is the $j$-th component of the mass flux vector $\mathbf{J}_n$ of species $n$, $q_j$ is the $j$-th component of the heat flux vector $\mathbf{q}$ and $\dot{\omega}_n$ is the mass-production rate of species $n$. Finally, $\tau_{ij}$ is the Newtonian viscous stress tensor

$$\tau_{ij} = \mu \left( \frac{\partial u_i}{\partial x_j} + \frac{\partial u_j}{\partial x_i} - \frac{2}{3} \frac{\partial u_k}{\partial x_k} \delta_{ij} \right), \tag{6}$$

where $\mu$ is the dynamic viscosity of the mixture and $\delta_{ij}$ is the Kronecker delta. In the present equations, body forces have been neglected.

Letting $\mathbf{F}^i = [F^i_m]\,(m = 1, \ldots, N+4)$ denote the flux vector of the conservative variables along the $i$-th direction, i.e.

$$\mathbf{F}^i \equiv [\rho u_i, \rho u_1 u_i + p\delta_{1i}, \rho u_2 u_i + p\delta_{2i}, \rho u_3 u_i + p\delta_{3i}, \rho u_i Y_1, \ldots, \rho u_i Y_{N-1}, (\rho e_t + p) u_i]^T, \tag{7}$$

the NS equations can be cast in compact form as

$$\frac{\partial \widetilde{\mathbf{U}}}{\partial t} + \frac{\partial \mathbf{F}^i}{\partial x_i} = \widetilde{\mathbf{C}}, \tag{8}$$

where the vector $\widetilde{\mathbf{C}} = [C_m]\,(m = 1, \ldots, N+4)$ is defined as

$$\widetilde{\mathbf{C}} \equiv [0, \frac{\partial \tau_{1j}}{\partial x_j}, \frac{\partial \tau_{2j}}{\partial x_j}, \frac{\partial \tau_{3j}}{\partial x_j}, -\frac{\partial J_{1j}}{\partial x_j} + \dot{\omega}_1, \ldots, -\frac{\partial J_{N-1j}}{\partial x_j} + \dot{\omega}_{N-1}, -\frac{\partial q_j}{\partial x_j} + \frac{\partial (\tau_{ij} u_i)}{\partial x_j}]^T. \tag{9}$$

When $\widetilde{\mathbf{C}} = \mathbf{0}$, one obtains the compressible Euler equations augmented by the species equations.

### B. The expressions for the heat, mass fluxes and viscosity of the mixture

Here we employ the generalized heat and mass transport equations based on the fluctuation-dissipation theory[11–13]. The mixing rules employed for the computation of the mass diffusion coefficients and thermal diffusion factors have been derived by Harstad & Bellan[14] and are based on the coupling of nonequilibrium thermodynamics[11] and Grad's 13-moment theory[15].

In the above setting, having neglected the term proportional to $\nabla p/p$ since it is anticipated that its contribution is minimal, the mass flux vector of species $n$ reads

$$\mathbf{J}_n = -\rho \left[ \sum_k (D_{nk} - D_n) \frac{M_n}{M_k} \nabla Y_k + Y_n D_{T,n} \frac{\nabla T}{T} \right], \tag{10}$$

where $M_n$ is species n molar mass, $D_{nk}$ are the pairwise mass diffusion coefficients and

$$D_{nk} = \sum_l a_{Dlk} D^M_{nl} \qquad D_{T,n} = -\sum_k \bar{a}^b_{T,k} D^M_{kn}, \tag{11}$$

$$D_n = \sum_k D_{nk} X_k \qquad \bar{a}^b_{T,n} = \sum_{k \neq n} X_k a^b_{T,kn}, \tag{12}$$

where $X_k$ is the mole fraction of species $k$, $a^b_{T,kn}$ are the binary thermal diffusion factors and $a_{Dnk}$ are the mass diffusion factors which are calculated in conjunction with the EOS as

$$a_{Dnk} = \frac{\partial X_n}{\partial X_k} + X_n \frac{\partial \ln \gamma_n}{\partial X_k}, \tag{13}$$

with $\gamma_n = \phi_n / \phi^o_n$, where $\phi_n$ is the fugacity coefficient of species $n$ and the superscript o denotes the single species ($X_n = 1$) limit. The elements $D^M_{kn}$ are obtained as the solution of the mixing rules equations

$$\sum_n \left[ \delta_{kn} - (1 - \delta_{kn}) X_n \frac{\bar{D}^b_k}{D^b_{kn}} \right] \frac{D^M_{nl}}{X_n} = \bar{D}^b_k \frac{(\delta_{kl} - Y_k)}{X_k}, \tag{14}$$

where

$$\bar{D}^b_k = \frac{1}{\sum_{n \neq k} \frac{X_n}{D^b_{kn}}}, \tag{15}$$

and where $D^b_{kn}$ is the full-approximation binary diffusivity. A solution for $D^M_{kn}$ can be obtained through an approximate inversion[16] as follows

$$D^M_{kn} \approx X_k D^{(1)}_{kn}, \tag{16}$$

where

$$D^{(1)}_{kn} = \left( \frac{1 + Y_k}{X_k} \right) D^*_k \delta_{kn} + (1 - \delta_{kn}) \frac{D^*_k D^*_n}{D^b_{kn}} - (\sigma_k D^*_k + \sigma_n D^*_n) + \sum_l Y_l \sigma_l D^*_l, \tag{17}$$

$$D^*_k = (1 - Y_k) \bar{D}^b_k, \tag{18}$$

$$\sigma_k = \frac{M_k}{M} (1 + Y_k) + \sum_{n \neq k} Y_n \frac{D^*_n}{D^b_{kn}}, \tag{19}$$

and where $M$ is the mixture's molar mass. To avoid in the above method artificial singularities for mixtures with vanishing mass-fractions, we follow the procedure of the EGLIB multicomponent transport property library[17,18]. To this end, we first calculate perturbed mole fractions as

$$X^{per}_n = X_n + \epsilon \left( \frac{\sum_n X_n}{N} - X_n \right), \tag{20}$$

where $\epsilon = 10^{-16}$ is a small parameter. Then we evaluate the perturbed molar mass of the mixture $M^{per} = \sum_n X^{per}_n M_n$ and finally the perturbed mass fractions as

$$Y^{per}_n = \frac{M_n}{M^{per}} X^{per}_n. \tag{21}$$

The heat flux vector reads

$$\mathbf{q} = -\lambda \nabla T + \sum_k (h_k - R_u T \bar{a}^b_{T,k}) \frac{\mathbf{J}_k}{M_k}, \tag{22}$$

where $\lambda$ is the thermal conductivity, $R_u$ the universal gas constant and $h_k$ the partial molar enthalpy of species $k$.

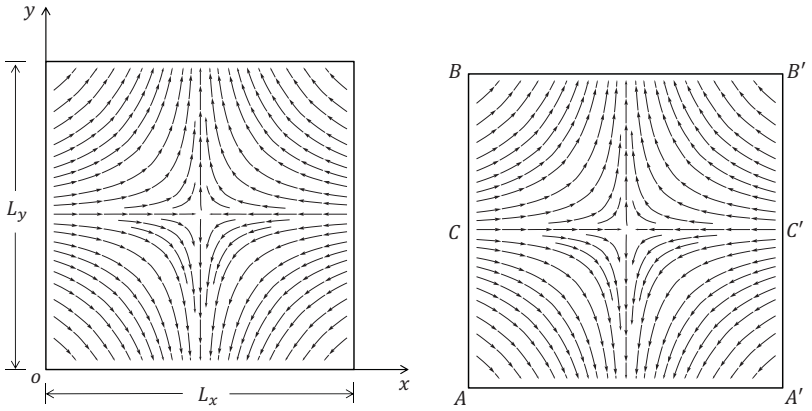


**Figure 1. The initial potential flow entering through the left $AB$ and right $A'B'$ inlet boundaries and exiting through the lower $AA'$ and $BB'$ boundaries. The solid lines represent the streamlines and the arrows the direction of the flow.**

### C. Transport properties

Transport properties were computed according to the most up-to-date methods[14,19–21].

### D. Equation of state

All NS equations are coupled with an EOS which is selected here to be the Peng-Robinson (PR) EOS[22]

$$p = \frac{R_u T}{v_{PR} - b_{mix}} - \frac{a_{mix}}{v_{PR}^2 + 2 b_{mix} v_{PR} - b_{mix}^2} \tag{23}$$

from which $T$ and $p$ are obtained as an iterative solution of two nonlinear equations that satisfy both the values of $\rho$ and $e$ as obtained from the solution of the conservation equations. In the PR EOS, $v_{PR}$ is the PR molar volume and it holds $v = v_{PR} + v_s$ where $v_s$ is the volume shift that improves the accuracy of the PR EOS for high-pressure conditions[23], while the terms $a_{mix}$ and $b_{mix}$ are functions of $T$ and $X_i$.

## III. Initial profile: Inviscid incompressible potential flow

The initial flow is a two-dimensional potential flow in which two opposing streams, each of constant density and composition, are injected from the two boundaries $AB$ and $A'B'$ of length $L_y$ in the $x$-direction; the streams exit the domain through the two boundaries $AB$ and $A'B'$ of length $L_x$ at the $y$-direction as illustrated in Fig. (1). At the point $C$ of the left inlet boundary, reference inflow variables $\rho^l_{ref}, T^l_{ref}, Y^l_{i,ref}$ and $p^l_{ref}$ are specified and their values are constant with time. Similarly, at the point $C'$ of the right inlet boundary, reference constant in time inflow variables $\rho^r_{ref}, T^r_{ref}, Y^r_{i,ref}$ and $p^r_{ref}$ are specified. The reference pressures at the two inlets are set equal, i.e. $p^l_{ref} = p^l_{ref} = p_{ref}$, so that for the initial flow described in the following, the stagnation point (S) is always located at the centerline with $x_S = L_x/2$ and also $y_S = L_y/2$.

The density field is given as

$$\rho^0(x,y) = \begin{cases} \rho^l_{ref} & \text{if} \quad 0 \le x < L_x/2, \forall y \\ \rho^r_{ref} & \text{if} \quad L_x/2 < x \le L_x, \forall y \end{cases}, \tag{24}$$

where a discontinuity arises to $\rho^0(x,y)$ at $x = L_x/2, \forall y$ when $\rho^l_{ref} \neq \rho^r_{ref}$. The species initial mass fraction fields are given as

$$Y^0_n(x,y) = \begin{cases} Y^l_{n,ref} & \text{if} \quad 0 \le x < L_x/2, \forall y \\ Y^r_{n,ref} & \text{if} \quad L_x/2 < x \le L_x, \forall y \end{cases}, \tag{25}$$

with $n = 1, \ldots, N$ and a discontinuity arises to $Y_n^0(x,y)$ at $x = L_x/2, \forall y$ when $Y_{n,ref}^l \neq Y_{n,ref}^r$. The components of the initial velocity field are

$$u_x^0(x,y) = -\frac{2\kappa(x - L_x/2)}{1 + \sqrt{\rho_{ref}^l/\rho_{ref}^r}}, \tag{26}$$

$$u_y^0(x,y) = \frac{2\kappa(y - L_y/2)}{1 + \sqrt{\rho_{ref}^l/\rho_{ref}^r}}, \tag{27}$$

for $0 \leq x < L_x/2, \forall y$, while for $L_x/2 < x \leq L_x, \forall y$ are

$$u_x^0(x,y) = -\frac{2\kappa(x - L_x/2)}{1 + \sqrt{\rho_{ref}^r/\rho_{ref}^l}}, \tag{28}$$

$$u_y^0(x,y) = \frac{2\kappa(y - L_y/2)}{1 + \sqrt{\rho_{ref}^r/\rho_{ref}^l}}, \tag{29}$$

where $\kappa$ is the strain rate. $u_x^0(x,y)$ is continuous $\forall(x,y)$, while $u_y^0(x,y)$ has a discontinuity at $x = L_x/2, \forall y$ when $\rho_{ref}^l \neq \rho_{ref}^r$.

Using (i) the common reference pressure, $p_{ref}$, of points $C$ and $C'$, (ii) the Bernoulli equation which holds for inviscid incompressible flows and (iii) the fact that for irrotational (i.e. potential) flows the total pressure, as given by the Bernoulli equation, is the same for all points of the flow (otherwise the Bernoulli equation would only hold along a streamline), we obtain the initial pressure field, $p^0$, as

$$p^0(x,y) = p_{ref} + \frac{1}{2}\rho_{ref}^l \left[ \left(u_x^0(x_C, y_C)\right)^2 + \left(u_y^0(x_C, y_C)\right)^2 \right] - \frac{1}{2}\rho_{ref}^l \left[ \left(u_x^0(x,y)\right)^2 + \left(u_y^0(x,y)\right)^2 \right], \tag{30}$$

for $0 \leq x < L_x/2, \forall y$, where $x_C = 0$ and $y_C = L_y/2$, while for $L_x/2 < x \leq L_x, \forall y$, $p^0$ is given by

$$p^0(x,y) = p_{ref} + \frac{1}{2}\rho_{ref}^r \left[ \left(u_x^0(x_{C'}, y_{C'})\right)^2 + \left(u_y^0(x_{C'}, y_{C'})\right)^2 \right] - \frac{1}{2}\rho_{ref}^r \left[ \left(u_x^0(x,y)\right)^2 + \left(u_y^0(x,y)\right)^2 \right], \tag{31}$$

where $x_{C'} = L_x$ and $y_{C'} = L_y/2$.

By construction, the initial potential flow satisfies the steady-state incompressible Euler's equations which in "compressible" form can be expressed as

$$\frac{\partial(\rho^0 u_x^0)}{\partial x} + \frac{\partial(\rho^0 u_y^0)}{\partial y} = 0 \tag{32}$$

$$\frac{\partial(\rho^0 u_x^0 u_x^0)}{\partial x} + \frac{\partial(\rho^0 u_x^0 u_y^0)}{\partial y} + \frac{\partial p^0}{\partial x} = 0 \tag{33}$$

$$\frac{\partial(\rho^0 u_x^0 u_y^0)}{\partial x} + \frac{\partial(\rho^0 u_y^0 u_y^0)}{\partial y} + \frac{\partial p^0}{\partial y} = 0 \tag{34}$$

$$\frac{\partial(\rho^0 Y_n^0 u_x^0)}{\partial x} + \frac{\partial(\rho^0 Y_n^0 u_y^0)}{\partial y} = 0 \quad (n = 1, \ldots, N-1) \tag{35}$$

$\forall x, y$ except for the locations at the interface line of the two streams, i.e. the points with $x_S = L_x/2, \forall y$. Equations (32)-(35) will be used next as a basis for constructing inflow boundary conditions for the NS equations. The availability of $p^0(x,y), \rho^0(x,y), Y_1^0(x,y), \ldots, Y_N^0(x,y)$ in conjunction with the EOS allows the determination of the initial temperature field of the flow, $T^0(x,y)$, by solving

$$p^0(x,y) = p(T^0(x,y), \rho^0(x,y), Y_1^0(x,y), \ldots, Y_N^0(x,y)) \tag{36}$$

for $T^0(x,y)$ where $p^0(x,y)$ is given by Eqs. (30)-(31), $\rho^0(x,y)$ is given by Eq. (24) and $Y_n^0(x,y)$ $(n = 1 \ldots, N)$ by Eq. (25). With the calculated $T^0(x,y)$, the initial specific internal energy field

$$e^0(x,y) = e(T^0(x,y), p^0(x,y), Y_1^0(x,y), \ldots, Y_N^0(x,y)) \tag{37}$$

of the flow is calculated as well. It follows that the initial field of conservatives variables, $\tilde{\mathbf{U}}^0(x,y)$, can then be readily constructed.

Finally, we note that for the counterflow configuration the use of a potential flow as initial flow is consistent with the fact that even when starting computations with a plug flow (i.e. zero y-components of the velocity vector at the inlets), the flow quickly converges to a potential type.

# IV. Boundary conditions

## A. Inflow boundary conditions

Instead of explicitly imposing timewise constant boundary values (also known as hard BCs) for the conservative variables at the two inlets $AB$ and $A'B'$, we impose the steady-state NS compressible conservation equations

$$\frac{\partial(\rho u_x)}{\partial x} + \frac{\partial(\rho u_y)}{\partial y} = 0 \tag{38}$$

$$\frac{\partial(\rho u_x u_x)}{\partial x} + \frac{\partial(\rho u_x u_y)}{\partial y} + \frac{\partial p}{\partial x} = \frac{\partial \tau_{xx}}{\partial x} + \frac{\partial \tau_{xy}}{\partial y} \tag{39}$$

$$\frac{\partial(\rho u_x u_y)}{\partial x} + \frac{\partial(\rho u_y u_y)}{\partial y} + \frac{\partial p}{\partial y} = \frac{\partial \tau_{yx}}{\partial x} + \frac{\partial \tau_{yy}}{\partial y} \tag{40}$$

$$\frac{\partial(\rho Y_n u_x)}{\partial x} + \frac{\partial(\rho Y_n u_y)}{\partial y} = -\frac{\partial J_{nx}}{\partial x} - \frac{\partial J_{ny}}{\partial y} + \dot{\omega}_n \quad (n = 1, \ldots, N-1) \tag{41}$$

for $\rho, \rho u_x, \rho u_y, \rho Y_1, \ldots, \rho Y_{N-1}$. Using these equations as BCs means that the initial values imposed on the inlets $AB$ and $A'B'$ for these variables are implicitly constrained to be constant with time. Most importantly, the transverse terms that give rise to multi-directional effects at the inflow boundaries are inherently present in the BCs. In addition to the above BCs, a simple algebraic equation of the form

$$\rho e_t = \rho \bar{e}_t(T(x,y), p(x,y), Y_1(x,y), \ldots, Y_N(x,y)) \tag{42}$$

is used for the boundary values of $\rho e_t$ at the two inlets, where $\bar{e}_t$ is calculated using the current values of $\rho, \rho u_x, \rho u_y, \rho Y_1, \ldots, \rho Y_{N-1}$ and calculating $T$ from the EOS and then $\bar{e}$, so that the values of $\rho \bar{e}_t$ are readily available.

By construction, the initial values of $\rho, \rho u_x, \rho u_y, \rho Y_1, \ldots, \rho Y_{N-1}$ at the inlets, as given by the potential flow of Section III, satisfy the Euler instead of the NS steady-state equations. Since the inlet boundaries are usually located away from the flame, these initial values provide a good initial guess for the NS steady-state equations which can be corrected[24] to account the viscous and species mass-flux effects.

## B. Outflow boundary conditions

At the outflow boundaries $A'A$ and $BB'$, the solution satisfies the unsteady NS equations since the conditions there are the outcome of the processes taking place in the interior of the domain. At these boundaries we assume that $p$ stays constant with time as initially provided by the Bernoulli equation.

# V. Numerical scheme

An eight-order explicit finite-difference scheme is used for the spatial derivatives. After spatially discretized, the steady-state NS equations become algebraic equations at a node, whereas the unsteady NS equations become ordinary differential equations at a node. As a result, at the nodes of the inflow boundaries $AB$ and $A'B'$, the BCs are of algebraic type since Eqs. (38)-(41) and Eq. (42) become algebraic equations. In addition, auxiliary ghost points can be used from the left of the boundary $AB$ and the right of the boundary $A'B'$ (since the solution is known there) to enhance the finite difference approximation of the spatial derivatives in Eqs. (38)-(41). At the nodes of outflow boundaries $A'A$ and $BB'$, the BCs are of differential type and one-sided finite differencing is used.

The resulting numerical system of differential-algebraic equations[25] is integrated in time with the differential-algebraic solver IDA of the SUNDIALS suite[26]. The integration method used in IDA is a variable-order, variable-coefficient BDF (Backward Differentiation Formula), in fixed-leading-coefficient form where the order of the method varies between 1 and 5. The BDF method can handle the stiffness introduced in the numerical integration of the NS equations due to the presence of chemical source terms. IDA supports parallel computations through the message passing interface (MPI) protocol and provides a routine that computes consistent initial conditions from a users' initial guess[24,27].

# VI. Reproducing non-reacting potential flows with the proposed differential-algebraic boundary conditions

To validate the proposed differential-algebraic BCs of Section IV, we consider two symmetric non-reacting potential flows where either $H_2$ or $O_2$ enters from both inlets. The goal is to numerically reproduce these two steady-state potential flows at computational times characteristic to reaction/diffusion problems.

**Table 1. The inflow conditions at the reference points $C$ and $C'$ of the left and right inlet (see the right part of Fig. (1)) used for the two symmetric $H_2$ potential flows cases A and B.**

| Case | Species | $\rho_{ref}$ (kg/m$^3$) | $T_{ref}$ (K) | $p_{ref}$ (bar) | $\kappa$ (s$^{-1}$) |
|---|---|---|---|---|---|
| A | $H_2$ | 0.08077 | 300 | 1 | $2 \times 10^3$ |
| B | $H_2$ | 0.08077 | 300 | 1 | $4 \times 10^3$ |

## A. The $H_2$ symmetric potential flow

For the symmetric $H_2$ potential flow, two situations are considered with different strain rates: case A with $\kappa = 2000$ s$^{-1}$ and case B with $\kappa = 4000$ s$^{-1}$. The inflow conditions are given on Table 1 and the size/meshing parameters of the computational domain used in each simulation case on Table 2.

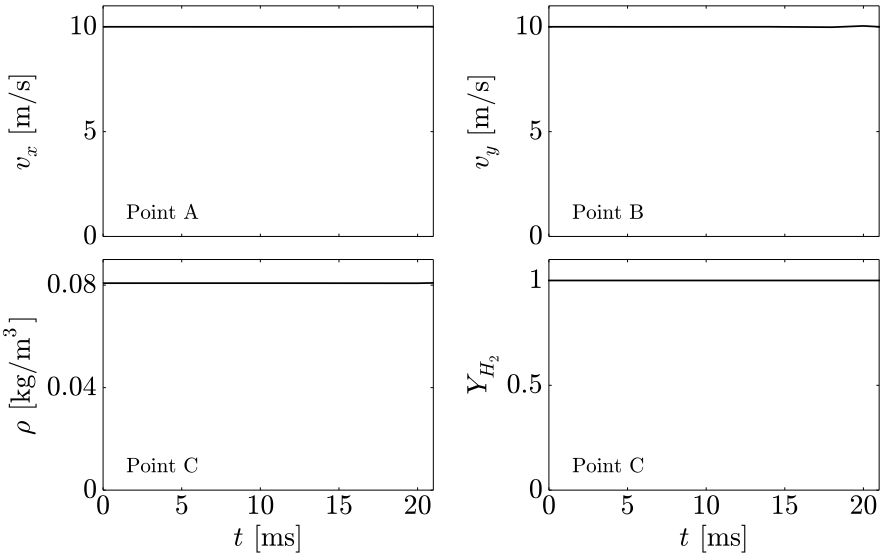


**Figure 2. Temporal variation of $\rho, v_x, v_y, p$ and $Y_{H_2}$ at inlet boundary points for Case A of the symmetric $H_2$ potential flow using the differential-algebraic BCs of Section IV. The inlet conditions are shown on Table 1, the size/meshing parameters of the computational domain on Table 2 and the labeling of the points refers to the right part of Fig. (1).**

Regarding case A, Fig. 2 shows the temporal evolution of the boundary values of $\rho, v_x, v_y$ and $Y_{H_2}$ at points on the left inlet boundary. The prescribed initial boundary values are excellently maintained by the imposed NS steady-state BCs, Eqs. (38)-(41), at the two inlets $AB$ and $A'B'$. Moreover, Fig. 4 shows the initial ($t = 0$ ms) spatial variation of $\rho, v_x, v_y, p$ and $Y_{H_2}$ for $x$-sections of the computational domain and the spatial variation of the same variables obtained at $t = 16$ ms. Clearly, the steady-state potential flow is accurately reproduced numerically in all respects.

Displayed in Figs. 3 and 5 are the equivalent results for Case B. The results for Case B are equally excellent in that the potential flow is maintained even for the larger $\kappa$ value.

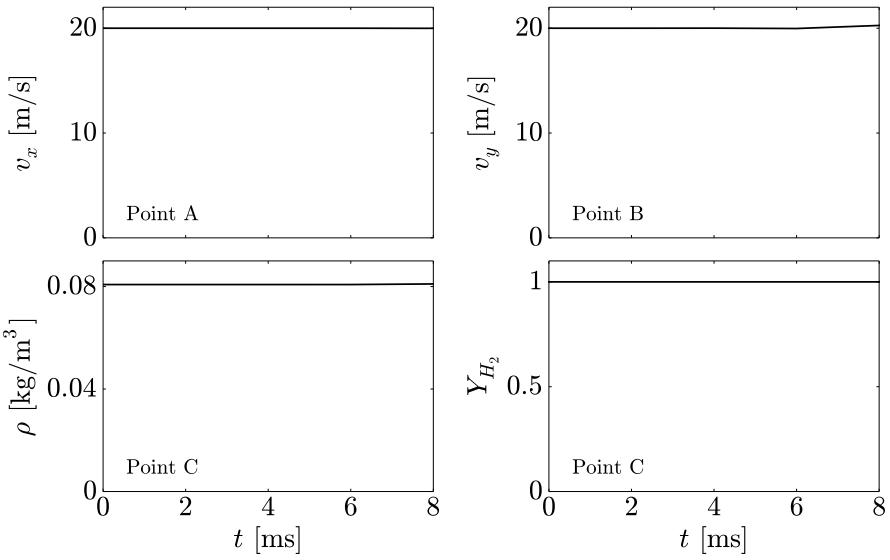


**Figure 3. Temporal variation of $\rho, v_x, v_y, p$ and $Y_{H_2}$ at inlet boundary points for Case B of the symmetric $H_2$ potential flow using the differential-algebraic BCs of Section IV. The inlet conditions are shown on Table 1, the size/meshing parameters of the computational domain on Table 2 and the labeling of the points refers to the right part of Fig. (1).**

**Table 2. The lengths $L_x$ and $L_y$ of the computational domain (see the left part of Fig. (1)) and the number of discretization points $N_x$ and $N_y$ at each direction used for the simulations of the two symmetric $H_2$ potential flows cases A and B.**

| Case | $L_x$ [mm] | $L_y$ [mm] | $N_x$ | $N_y$ |
|---|---|---|---|---|
| A | 10 | 10 | 104 | 104 |
| B | 10 | 10 | 144 | 144 |

### B. The $O_2$ symmetric potential flow

For the symmetric $O_2$ potential flow one situation is considered only. The inflow conditions are given on Table 3 and the size/meshing parameters of the computational domain used in the simulation on Table 4. The results of the simulation for $O_2$ are illustrated in Figs. 6 and 7 which represent a simulation performed with a fluid having a density of $\mathcal{O}(10)$ larger compared to that of $H_2$ used in the previous two simulations. The same high fidelity in maintaining numerically the imposed initial potential flow holds as in the $H_2$ simulations.

## VII. Summary and conclusions

New BCs have been developed for the counterflow configuration which provide a very concise framework that inherently accounts the multi-directional character of the flow at the boundaries. Upon discretization

**Table 3. The inflow conditions at the reference points $C$ and $C'$ of the left and right inlet (see the right part of Fig. (1)) used for the symmetric $O_2$ potential flow.**

| Species | $\rho_{ref}$ (kg/m$^3$) | $T_{ref}$ (K) | $p_{ref}$ (bar) | $\kappa$ (s$^{-1}$) |
|---|---|---|---|---|
| $O_2$ | 1.2837 | 300 | 1 | $2 \times 10^3$ |

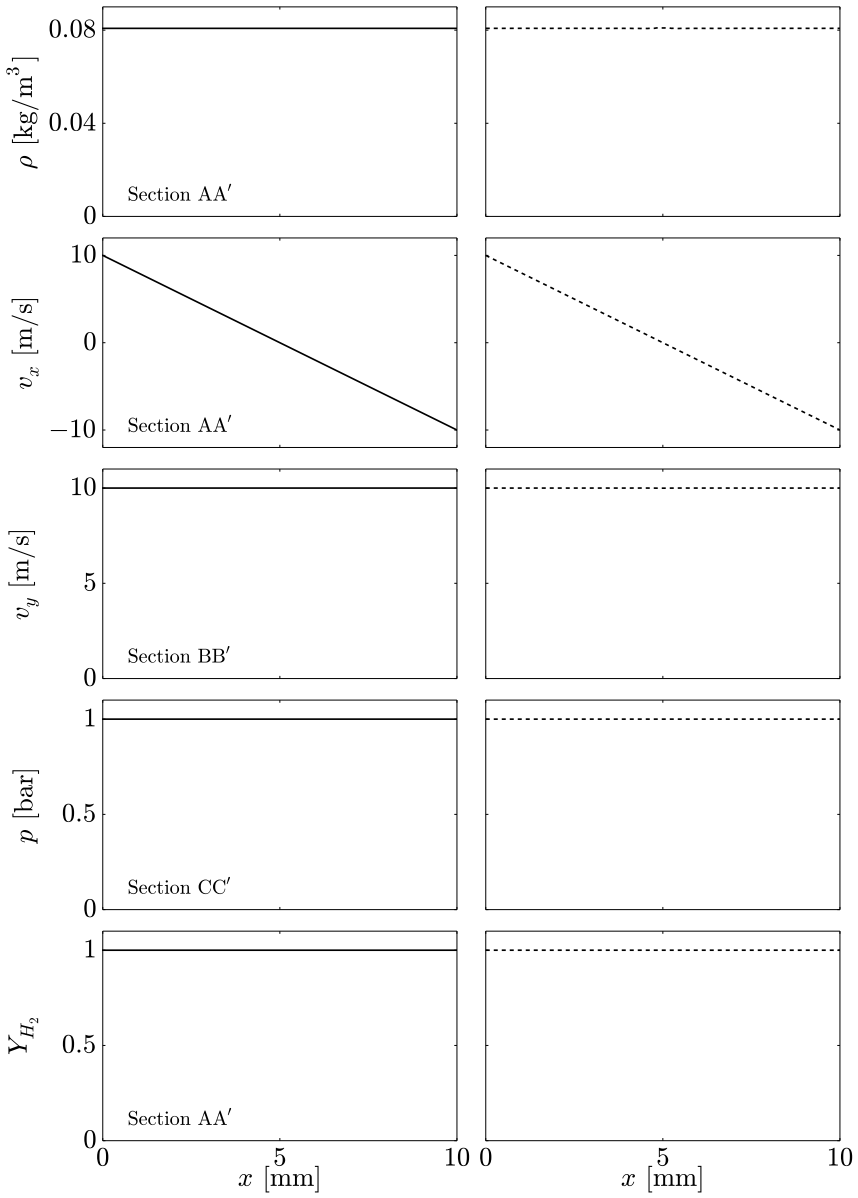


**Figure 4. Spatial variation of $\rho, v_x, v_y, p$ and $Y_{H_2}$ for Case A of the symmetric $H_2$ potential flow using the differential-algebraic BCs of Section IV. The inlet conditions are shown on Table 1, the size/meshing parameters of the computational domain on Table 2 and the labeling of the sections refers to the right part of Fig. (1). Left column: $t = 0$ ms. Right column: $t = 16$ ms.**

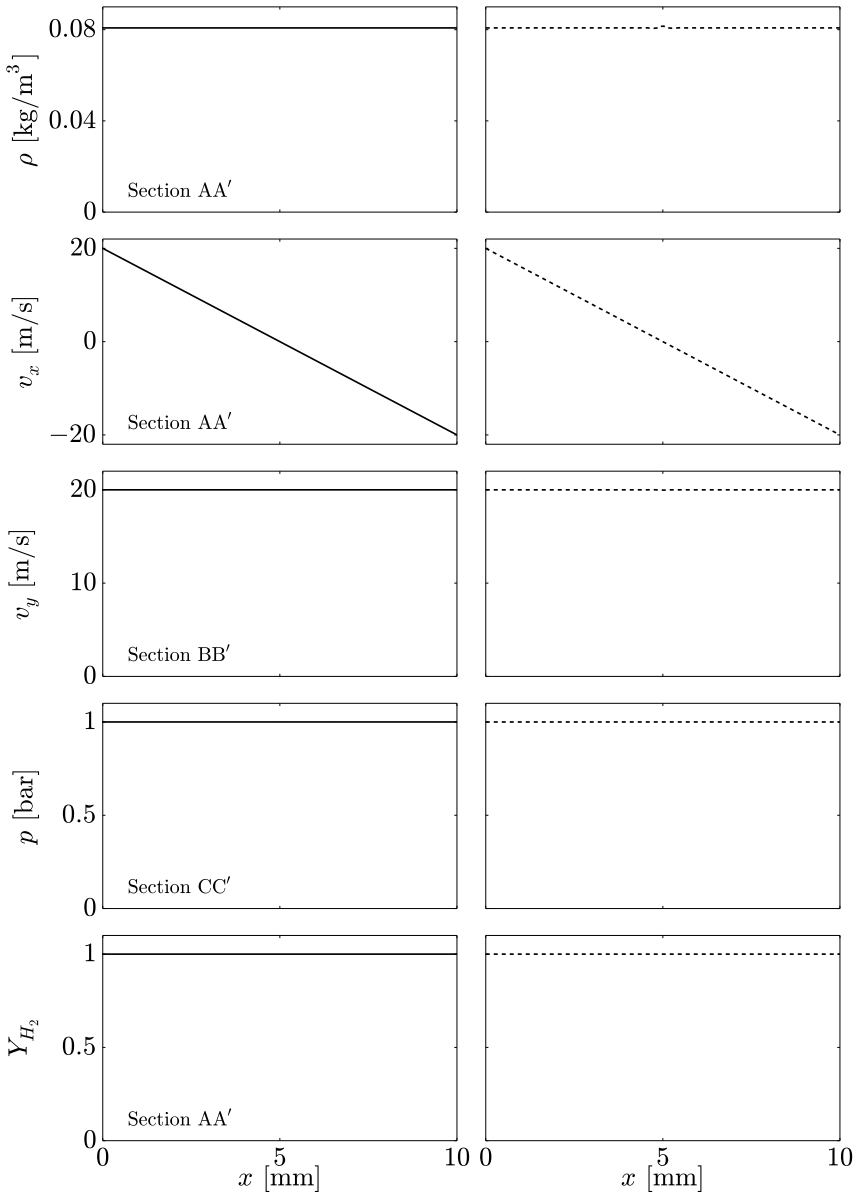


**Figure 5. Spatial variation of $\rho, v_x, v_y, p$ and $Y_{H_2}$ for Case A of the symmetric $H_2$ potential flow using the differential-algebraic BCs of Section IV. The inlet conditions are shown on Table 1, the size/meshing parameters of the computational domain on Table 2 and the labeling of the sections refers to the right part of Fig. (1). Left column: $t = 0$ ms. Right column: $t = 6$ ms.**

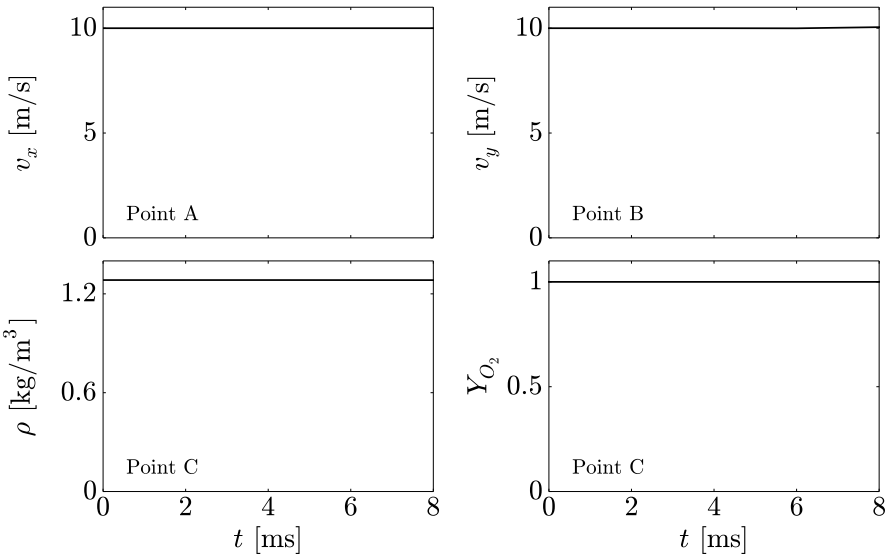


**Figure 6. Temporal variation of $\rho, v_x, v_y, p$ and $Y_{H_2}$ at inlet boundary points for the symmetric $O_2$ potential flow using the differential-algebraic BCs of Section IV. The inlet conditions are shown on Table 3, the size/meshing parameters of the computational domain on Table 4 and the labeling of the points refers to the right part of Fig. (1).**

**Table 4. The lengths $L_x$ and $L_y$ of the rectangular computational domain (see the left part of Fig. (1)) and the number of discretization points $N_x$ and $N_y$ at each direction used for the simulation of the symmetric $O_2$ potential flow.**

| $L_x$ [mm] | $L_y$ [mm] | $N_x$ | $N_y$ |
|---|---|---|---|
| 10 | 10 | 200 | 200 |

of the steady-state NS equations, the BCs at the inflow boundaries are of algebraic type, whereas upon discretization of the unsteady NS equations, those at the outflow boundaries are of differential type. This formulation of the numerical BCs as differential-algebraic ones requires the use of a numerical integration software capable of handling initial-value problems for differential-algebraic systems of equations such as the IDA of the SUNDIALS suite[26].

For the validation of the differential-algebraic BCs two symmetric non-reacting potential flows were considered with either $H_2$ or $O_2$ as injected species from both inlets. For $H_2$, two different strain rates cases where examined. One with $\kappa = 2000\,\mathrm{s}^{-1}$ which corresponded to an injection velocity of 10 m/s and one with $\kappa = 4000\,\mathrm{s}^{-1}$ which corresponds to an injection velocity of 20 m/s. For $O_2$, a single case was examined with $\kappa = 2000\,\mathrm{s}^{-1}$ which corresponds to an injection velocity of 10 m/sec. In all simulated cases, the BCs were able to maintain accurately the imposed boundary values at the inlet boundaries. Moreover, the initial potential flow was reproduced with high fidelity over the entire computational domain without numerical artifacts. For the aforementioned cases studied, there was no use of dissipative filters and there was no need of introducing relaxation constants into the BCs.

Reactive counterflow simulations with the differential-algebraic BCs are currently being conducted and will be the subject of a future publication.

## Acknowledgments

This work was performed at the California Institute of Technology and the Jet Propulsion Laboratory Division of the California Institute of Technology, and was sponsored by United States Army Research Office,

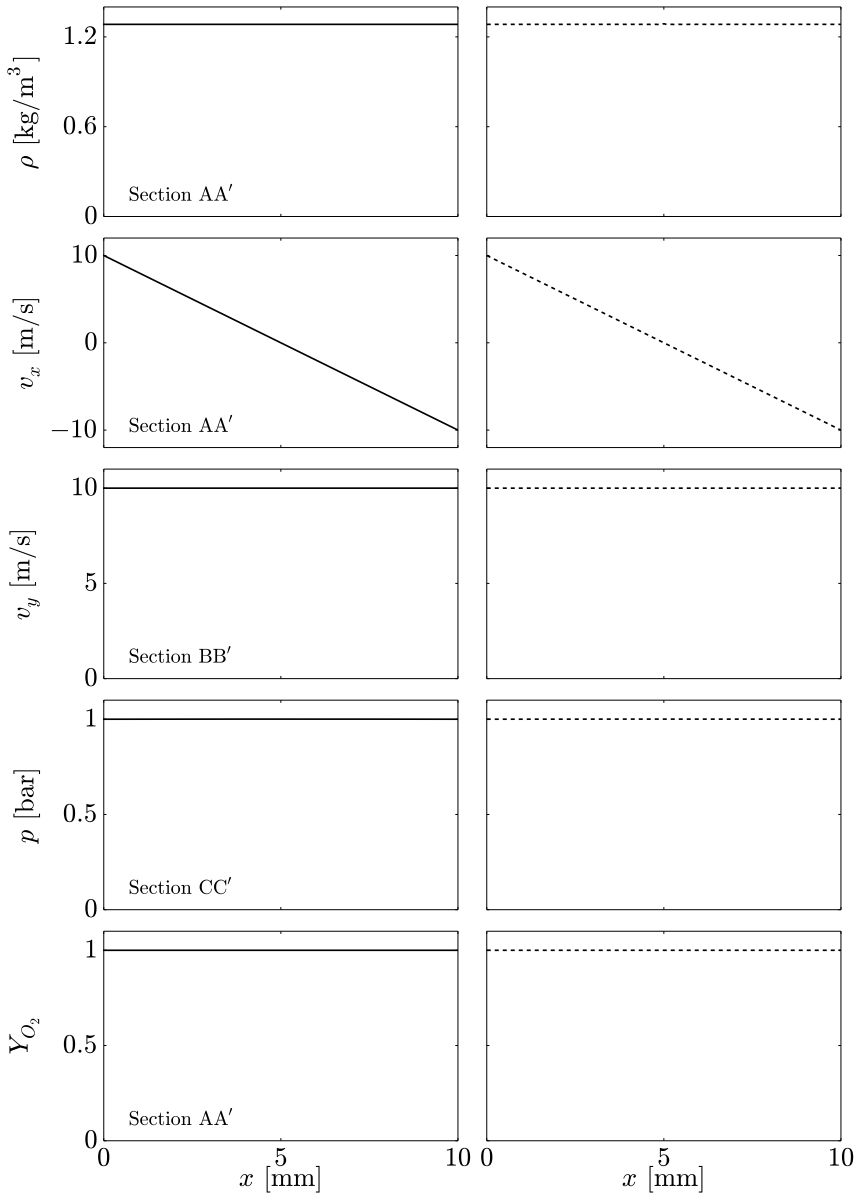


**Figure 7. Spatial variation of $\rho, v_x, v_y, p$ and $Y_{O_2}$ for a symmetric $O_2$ potential flow using the differential-algebraic BCs of Section IV. The inlet conditions are shown on Table 3, the size/meshing parameters on Table 4 and the labeling of the sections refers to the right part of Fig. (1). Left column: $t = 0$ ms. Right column: $t = 6$ ms.**

with Dr. Ralph Anthenien as contract monitor. Supercomputing time from the DoD HPCMP Open Research Systems and JPL/NASA is gratefully acknowledged.

## References

[1]Tsuji, H.,"Counterow diffusion flames," Prog. Energ. Combust., Vol. 8, No. 2, 1982, pp. 93-119.

[2]Mastorakos, E., Taylor, A., and Whitelaw, J., "Scalar dissipation rate at the extinction of turbulent counterflow non-premixed flames," Combust. and Flame, Vol. 91, No. 1, 1992, pp. 55-64.

[3]Seiser, R., Pitsch, H., Seshadri, K., Pitz, W., and Gurran, H., "Extinction and autoignition of n-heptane in counterflow configuration," P. Combust. Inst., Vol. 28, No. 2, 2000, pp. 2029-2037.

[4]Ribert, G., Zong, N., Yang, V., Pons, L., Darabiha, N., and Candel, S., "Counterflow diffusion flames of general fluids: Oxygen/hydrogen mixtures," Combust. and Flame, Vol. 154, No. 3, 2008, pp. 319-330.

[5]Agathou, M. S. and Kyritsis, D. C., "An experimental comparison of non-premixed bio-butanol flames with the corresponding flames of ethanol and methane," Fuel , Vol. 90, No. 1, 2011, pp. 255-262.

[6]Lacaze, G. and Oefelein, J. C., "A non-premixed combustion model based on flame structure analysis at supercritical presures," Combust. and Flame, Vol. 159, No. 6, 2012, pp. 2087-2103.

[7]Yoo, C. S., Wang, Y., Trouvé, A., and Im, H. G., "Characteristic boundary conditions for direct simulations of turbulent counterflow flames," Combust. Theory Model., Vol. 9, No. 4, 2005, pp. 617-646.

[8]Sarnacki, B. G., Esposito, G., Krauss, R. H. and Chelliah, H. K., "Extinction limits and associated uncertainties of nonpremixed counterflow flames for methane, ethylene, propylene and n-butane in air," Combust. and Flame, Vol. 159, 2012, pp. 1026-1043.

[9]Johnson, R. F., VanDine, A. C., Esposito, G. L. and Chelliah, H. K., "On the axisymmetric counterflow flame simulations: Is there an optimal nozzle diameter and separation distance to apply quasi one-dimensional theory?," Comb. Sci. Techn., Vol. 187, 2015, 1-23.

[10]Poinsot, T. J. and Lele, S. K., "Boundary conditions for direct simulations of compressible viscous flows," J. Comput. Phys., Vol. 101, No. 1, 1992, pp. 104-129.

[11]Keizer, J., Statistical Thermodynamics of Nonequilibrium Processes, Springer-Verlag, New York, 1987.

[12]Harstad, K. and Bellan, J., "Isolated fluid oxygen drop behavior in fluid hydrogen at rocket chamber pressures," Int. J. Heat Mass Tran., Vol. 41, No. 22, 1998, pp. 3537-3550.

[13]Harstad, K. and Bellan, J., "An all-pressure fluid drop model applied to a binary mixture: heptane in nitrogen," Int. J. Multiphas. Flow , Vol. 26, No. 10, 2000, pp. 1675-1706.

[14]Harstad, K. and Bellan, J., "Mixing rules for multicomponent mixture mass diffusion coefficients and thermal diffusion factors," J. Chem. Phys., Vol. 120, No. 12, 2004, pp. 5664-5673.

[15]Grad, H., "On the kinetic theory of rarefied gases," Commun. Pur. Appl. Math., Vol. 2, No. 4, 1949, pp. 331-407.

[16]Ern, A. and Giovangigli, V., "Thermal diffusion effects in hydrogen-air and methane-air flames," Combust. Theory Model., Vol. 2, No. 4, 1998, pp. 349-372.

[17]Ern, A. and Giovangigli, V., Multicomponent Transport Algorithms, Vol. 24 of Lecture Notes in Physics Monographs, Springer-Verlag, 1994.

[18]Ern, A. and Giovangigli, V., "EGLIB: a General-Purpose Fortran Library for Multicomponent Transport Property Evaluation," Tech. Rep. 96-51, CERMICS Internal Report, 1996.

[19]Reid, R. C., Prausnitz, J. M., and Poling, B. E., The properties of gases and liquids, McGraw Hill, 4th edition, 1987.

[20]Harstad, K. and Bellan, J., "High-Pressure Binary Mass Diffusion Coefficients for Combustion Applications," Ind. Eng. Chem. Res., Vol. 43, No. 2, 2004, pp. 645-654.

[21]Hirshfelder, J. O., Curtis, C. F., and Bird, R. B., Molecular Theory of Gases and Liquids, John Wiley & Sons Inc., 1954.

[22]Peng, D.-Y. and Robinson, D., "A new two-constant equation of state," Ind. Eng. Chem. Res., Vol. 15, No. 1, 1976, pp. 59-64.

[23]Harstad, K., Miller, R. S., and Bellan, J., "Efficient high-pressure state equations," AIChE J., Vol. 43, No. 6, 1997, pp. 1605-1610.

[24]Brown, P. N., Hindmarsh, A. C., and Petzold, L. R., "Consistent Initial Condition Calculation for Differential-Algebraic Systems," SIAM J. Sci. Comput., Vol. 19, No. 5, 1998, pp. 1495-1512.

[25]Brenan, K. E., Campbell, S. L., and Petzold, L. R., Numerical Solution of Initial-Value Problems in Differential-Algebraic Equations, SIAM, 1996.

[26]Hindmarsh, A. C., Brown, P. N., Grant, K. E., Lee, S. L., Serban, R., Shumaker, D. E., and Woodward, C. S., "SUNDIALS: Suite of Nonlinear and Differential/Algebraic Equation Solvers," ACM Trans. Math. Softw., Vol. 31, No. 3, 2005, pp. 363-396.

[27]Hindmarsh, A. C., Serban, R., and Collier, A., "User Documentation for IDA v2.7.0," Tech. Rep. UCRL-SM-208112, Lawrence Livermore National Laboratory, Livermore, CA, 2012.